metals

MDPI

Article

Structure–Phase Transitions in the Friction Contact Zone of High-Nitrogen Chromium–Manganese Austenitic Steel

Valery Shabashov [1,*], Lev Korshunov [1], Kirill Kozlov [1], Kirill Lyashkov [1], Andrey Zamatovskii [1], Gennady Dorofeev [2] and Natalya Kataeva [1]

[1] M.N. Mikheev Institute of Metal Physics, Ural Branch, Russian Academy of Sciences, 620108 Ekaterinburg, Russia; korshunov@imp.uran.ru (L.K.); kozlov@imp.uran.ru (K.K.); lyashkov@imp.uran.ru (K.L.); zamatovsky@imp.uran.ru (A.Z.); kataeva@imp.uran.ru (N.K.)

[2] Udmurt Federal Research Center, Ural Branch, Russian Academy of Sciences, 426067 Izhevsk, Russia; gadorofeev@udman.ru

* Correspondence: shabashov@imp.uran.ru

Abstract: The influence of contact stresses on the phase and concentration composition of thin surface layers and wear products in the tribological contact zone of high-nitrogen $FeMn_{22}Cr_{18}N_{0.83}$ steel was studied using Mössbauer spectroscopy, X-ray structural analysis, and electron microscopy. It was shown that contact compressive stresses developing under the conditions of dry sliding friction in the surface layers (20–25 microns) resulted in the strain-induced dissolution of cellular precipitation products (nitrides Cr_2N) and increased the average content of nitrogen in austenite. Antiferromagnetic ordering in austenite caused by the precipitation of secondary nitrides with low chromium and nitrogen content was observed in tiny external layers (~0.1 microns) of the friction surface and products of steel adhesive wear. The effect of tension stresses in the friction contact zone on the formation of strain-induced martensite and nitrides with α''-$Fe_{16}N_2$ structures was established in the wear products.

Keywords: austenitic steels; nitrides; friction; surface; Mössbauer spectroscopy

check for updates

Citation: Shabashov, V.; Korshunov, L.; Kozlov, K.; Lyashkov, K.; Zamatovskii, A.; Dorofeev, G.; Kataeva, N. Structure–Phase Transitions in the Friction Contact Zone of High-Nitrogen Chromium–Manganese Austenitic Steel. *Metals* **2023**, *13*, 1433. https://doi.org/10.3390/met13081433

Academic Editor: Alain Pasturel

Received: 26 June 2023
Revised: 28 July 2023
Accepted: 31 July 2023
Published: 10 August 2023

Copyright: © 2023 by the authors. Licensee MDPI, Basel, Switzerland. This article is an open access article distributed under the terms and conditions of the Creative Commons Attribution (CC BY) license (https://creativecommons.org/licenses/by/4.0/).

1. Introduction

One of the most practically important performance characteristics of tool steels in conditions of friction is the property of wear resistance. The tribological behavior of metallic materials is mostly determined by structural transformations taking place in a zone of friction contact [1–6]. The presence of irregularities on a surface of a studied material under conditions of dry sliding friction results in the development of local regions of contact. Due to metal plastic deformation in the local region of true contact during sliding, the whole geometric surface of contact and the neighboring microvolumes of the material are involved in a deformation interaction [3]. Under particular parameters of friction exposure, the influence of contact stresses on a structure may be attributed to severe (mega) plastic deformation [7–12]. High values of contact stresses have been supported by the results of polymorphous structure–phase transitions in metastable alloys of an Fe–Mn system under dry sliding friction and high-pressure torsion in rotating Bridgman anvils [3]. Compressive stresses in the friction contact zone are comparable with the material strength limit and reach 6–11 GPa. High-pressure torsion is believed to be a macro model of deformation in the friction contact zone [3]. The influence of friction on the structure of nitrogen-containing austenitic steel was studied in [8,10,12], applying transmission Mössbauer spectroscopy to foils with a thickness of 20–25 microns obtained via one-side thinning with an undamaged region affected by friction. In this case, the Mössbauer spectrum characterizes an average phase and concentration content within a sample thickness. The surface subjected to friction generally has a gradient structure, i.e., variation in plastic deformation influence between the surface layers and internal regions of the sample.

Today, nitrous chrome–manganese steels are considered to be the most promising austenitic steels with advanced wear properties [1–6,10–12]. The wear properties of tool steels are mostly defined by structural phase transformations in the surface layers of friction contact. Therefore, the goal of the current study was to examine the structure and composition of the sliding friction surface of austenitic chrome–manganese steel samples alloyed with nitrogen. The thin layers of the adhesive wear surface bordering with the contact stress zone are of great interest for study because the friction surface suffers the most significant exposure.

In particular, it was interesting to analyze the structure of wear products occurring after sample degradation in the region of the highest contact stresses.

2. Materials and Methods

The investigated material is represented by $FeMn_{22}Cr_{18}N_{0.83}$ (wt. %: 0.05 C, 22.1 Mn, 17.9 Cr, 0.83 N, and rest Fe) stainless austenitic steel melted out via countergravity casting with nitrogen. The steel was homogenized at 1100 °C followed by hot forging. Samples with a size of $7 \times 7 \times 20$ mm^3 were prepared from rods with a cross-section of 10×10 mm^2 quenched in water at 1150 °C. A part of the quenched samples was subjected to discontinuous precipitation by means of aging annealing at 800 °C. After thermal treatment, the operating surfaces of the samples (7×7 mm^2) were mechanically polished according to cleanness grade 8 (roughness: $\leq$0.5 microns). In order to analyze the structure of the $FeMn_{22}Cr_{18}N_{0.83}$ steel, a model austenitic alloy, $FeMn_{20}$, and mechanically synthesized steels obtained with the compositions Fe + 20%Mn_2N and $FeCr_{15}$ + 20%Mn_2N were used.

Friction tests were performed under conditions of dry sliding friction on steel–steel pairs in ambient air according to a finger plate scheme with sample–finger reciprocation movement. The plates were made of carbon steel and thermally treated up to 50 HRC hardness. The test conditions comprised a conventional load of 294 N, sliding velocity of 0.07 m/s, and sliding distance of 80 m. The sample temperature at 0.2–0.5 mm distance from the friction surface did not exceed 50 °C. The scheme of affection in conditions of dry sliding friction can be represented by a single sliding semispherical asperity, namely, a counterbody [3], as shown in Figure 1. Moving asperities formed compressive and stretching areas in the alloy surface layer. During friction action, the surface of the treated material was modified and even failed with the development of wear products in powder form. Both surface structures of the samples and wear products were investigated in the current study.

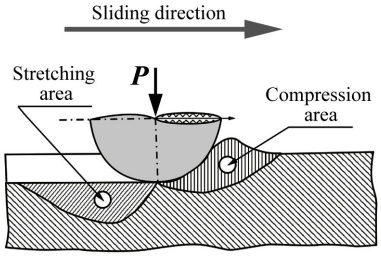


Figure 1. The scheme of irregularity effect (counterbody) illustrated as single, solid, smooth semisphere on the steel surface in conditions of dry sliding friction.

The methods used were Mössbauer spectroscopy, electron microscopy, and X-ray structural analysis. Mössbauer measurements in transmission geometry of 14.4 keV γ-rays were performed at room temperature (298 K) using an MS-1101 spectrometer (Research Institute of Physics SFedU, Rostov–on–Don, Russia) and ^{57}Co(Cr) resonance source. All spectra were calibrated in relation to α-Fe at room temperature. In the experiments, the surface layers of the samples prepared as 20–25-micron-thick foils by one-side thinning toward the friction contact, as well as powdered wear products, were studied. Moreover, Mössbauer spectroscopy on internal conversion electrons was also used, providing knowledge about the ~0.1-micron surface layers. Mössbauer spectra analysis was performed

using MS Tools software (Versions 6.1 and 7.2) [13]. The steel structure was investigated using Quanta 200 scanning electron microscope (FEI Company, Hillsboro, OR, USA) with accelerating voltage of ~30 kV and a JEM 200CX transmission electron microscope (JEOL, Tokyo, Japan) with accelerating voltage of ~160 kV in bright- and dark-field modes and microdiffraction regimes. X-ray structural analysis was performed using the following diffractometers: (i) Rigaku Miniflex 600 (Rigaku Corporation, Tokyo, Japan) in Co-Kα radiation; (ii) Empyrean (PANalytical, Almelo, The Netherlands) in Cu-Kα radiation. Approximation of obtained data was performed on the assumption of two-phase presence, using full-profile analysis software for X-ray diffraction patterns FullProf Suite (Version 2019.10.21-1).

3. Experimental Results

3.1. Analysis of the Sample Surface Subjected to Friction

According to electron microscopy data, the structure of the initial quenched $FeMn_{22}Cr_{18}N_{0.83}$ steel revealed no visible nitride precipitates. Steel aging at 800 °C for 2 and 30 h resulted in the breakdown of 40 and 90%, respectively, of solid solution with the development of pearlite-like cellular precipitation structures represented by interstratified austenite plates and chromium nitrides (Cr_2N) with thickness of ~30–50 nm [2,8,11], as shown in Figure 2a,c. For this structure, single-crystal microdiffraction is rather characteristic (see the insert in Figure 2a), with reflections from two correspondent phases with zone axis ZA $[001]_\gamma$ and ZA $[231]_{Cr2N}$.

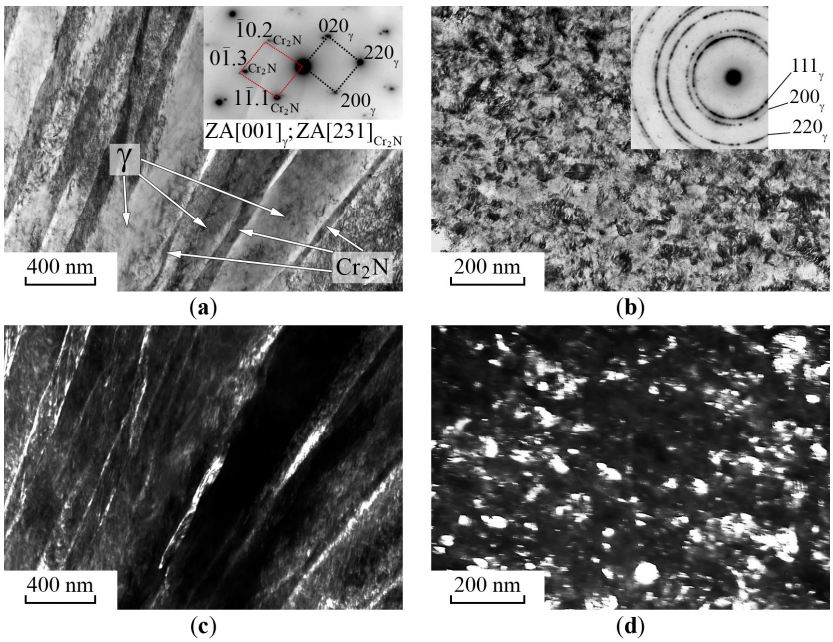


Figure 2. Electron microscopy of $FeMn_{22}Cr_{18}N_{0.83}$ steel structure. (**a**,**b**)—Bright-field images and SAED patterns; (**c**)—dark-field image of (**a**) registered in the complex reflection $((220)_\gamma + (01.\bar{3})_{Cr2N})$; (**d**)—dark-field image of (**b**) registered in the reflection $(200)_\gamma$. Treatment: (**a**,**c**)—aging 800 °C, 30 h; (**b**,**d**)—aging 800 °C, 30 h, and friction.

Dry sliding friction provides the formation of austenitic nanocrystalline structures in the surface layers at a depth of 5 μm, as shown in Figure 2b,d. The insert in Figure 2b shows microdiffraction, which contains ring reflections of strongly disoriented austenite grains. Reflections from Cr_2N nitrides were not revealed possibly due to their dissolution.

The Mössbauer spectra of $FeMn_{22}Cr_{18}N_{0.83}$ steel in the initial quenched condition and after aging and the friction test revealed the spectrum shape of paramagnetic austenite for the samples with one-side thinning [10,12], as shown in Figure 3. The calculation of intensity distribution for Mössbauer absorption vs. the Doppler velocity scale $p(V)$ illustrated the

spectra structure (see Figure 3a–c,a′–c′). The decomposition of $p(V)$ distribution using Gaussian lines allows for roughly representing an integral spectrum as a superposition of two doublets, $D0 + D1$. The presence of the doublet $D0$ was determined using an electric field gradient on ^{57}Fe nuclei formed by surrounding substitutional impurities (Mn and Cr). The hyperfine parameters of $D0$ (isomer shift, I_s, and quadrupole splitting, Q_s) are similar to those of the stainless steels [14,15]. The doublet $D1$ was caused by one interstitial nitrogen in the proximal octahedral interstices of resonant iron in the FCC crystal matrix, as shown in Table 1.

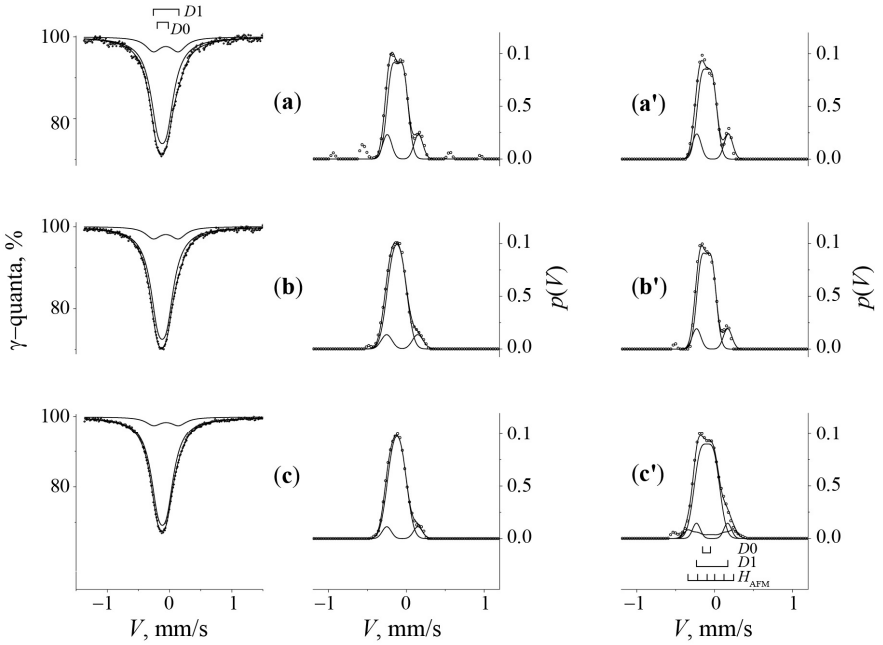


Figure 3. Mössbauer spectra and $p(V)$ distributions of $FeMn_{22}Cr_{18}N_{0.83}$ steel. Treatment: (**a**)—quenching from 1150 °C; (**b**)—aging 800 °C, 2 h; (**c**)—aging 800 °C, 30 h. (**a′**–**c′**)—$p(V)$ distribution functions after treatments (**a**–**c**) and friction, respectively.

Table 1. Mössbauer parameters of austenite spectra of the $FeMn_{22}Cr_{18}N_{0.83}$ steel in the 20–25 μm and ~0.1 μm surface layers and the wear products after tempering, aging, and dry sliding friction effect.

	Treatment *	*D*0			*D*1			H_{AFM}		
		I_S	Q_S	*S*	I_S	Q_S	*S*	I_S	*H*	*S*
1	Quenching	–0.12	0.14	80	–0.06	0.40	20	–	–	–
2	Aging 2 h	–0.12	0.14	87	–0.06	0.40	13	–	–	–
3	Aging 30 h	–0.12	0.12	90	–0.06	0.38	10	–	–	–
4	Quenching and aging 30 h	–0.10	0.14	79	–0.03	0.40	21	–	–	–
5	Aging 2 h and friction	–0.11	0.13	85	–0.03	0.40	15	–	–	–
6	Aging 30 h and friction	–0.10	0.16	75	–0.03	0.40	14	–0.05	19	11
7	Quenching, wear production	–0.10	0.14	70	–0.02	0.40	18	–0.04	21	4
8	Aging 2 h, wear production	–0.10	0.16	63	0.02	0.40	13	–0.03	22	16
9	Aging 30 h, wear production	–0.10	0.16	54	0.03	0.40	5	–0.03	22	20
10	Aging 30 h, CEMS	–0.11	0.00	90	–0.03	0.40	10	–	–	–
11	Aging 30 h and friction, CEMS	–0.11	0.10	73	–	–	–	0.02	21	27

* Numbers 1–9 indicate measurements using transmission Mössbauer spectroscopy; 10–11 indicate measurements using conversion electron Mössbauer spectroscopy (CEMS).

The hyperfine parameters of $D1$ were found to be similar to those of the doublet in the iron nitride spectrum [16]. The evaluation of the nitrogen content (c_N) in the $FeMn_{22}Cr_{18}N_{0.83}$ steel was performed on the assumption of the repulsive distribution

(repulsive interaction) of nitrogen atoms in a solid solution according to the contribution of the $D1$ configuration related to iron atoms with nitrogen in the proximal octahedral interstices (by relative integral intensity S_{D1} similar to [16]). The supposed spectra model for the studied steel was supported by results of quenching, further aging, and the influence of dry sliding friction or cold work by shear under pressure [10], as shown in Figure 3 and Table 1. The decreased relative intensity of the doublet $D1$ in the spectra of samples aged at 800 °C for 2 and 30 h indicated the nitrogen release from the interstitial solid solution to nitrides and the decreased nitrogen content (c_N) in the austenite from 2 to 1.3 and less than 1 at. %, respectively [10]. X-ray structural analysis revealed decreased lattice spacing from 0.3630 to 0.3614 nm, confirming the decreased nitrogen content in the FCC of the solid solution under the conditions of thermal aging.

The transmission Mössbauer spectra of the samples obtained by one-side thinning toward the tribological contact specified the mean integral characteristic of the effect over a foil thickness of about 20–25 μm. The spectra and $p(V)$ distributions of the quenched steel surface layers subjected to friction revealed no visible variations in the partial contribution value of $D1$, as shown in Figure 3a′ and Table 1. Consequently, sliding friction did not change the mean nitrogen content over a 20–25 μm thickness and the phase composition in the surface layers of the quenched steel.

The transmission Mössbauer spectra of the aged steel after friction revealed a singlet pattern related to the paramagnetic austenite but with a significantly increased proportion of the doublet component $D1$. This fact reflects the increased nitrogen content in the austenite (see Figure 3b′,c′ and Table 1). Using conversion electron Mössbauer spectroscopy (CEMS) on the steel samples provides information about the ~0.1 μm surface layers and some variations discussed further in Section 3.2 (see Figure 4).

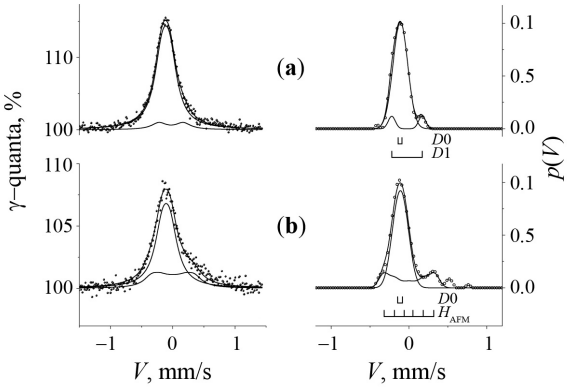


Figure 4. Conversion electron Mössbauer spectra (CEMS) and $p(V)$ distributions of $FeMn_{22}Cr_{18}N_{0.83}$ steel. Treatment: (**a**)—aging 800 °C, 30 h; (**b**)—aging 800 °C, 30 h and friction.

The results of the X-ray structural analysis confirm the increased nitrogen content in the solid solution after friction, as shown in Figure 5a,b. The diffraction pattern of the sample after friction revealed a gradient composition of the γ-phase with distinguishing lattice parameters caused by a variation in the alloying degree of layers throughout the depth. The layer thickness for X-ray analysis is several microns. The diffraction pattern demonstrated contributions from at least two layers with distinguishing concentrations of elements.

For this reason, the diffraction pattern can be fitted in the frame of a single-reflection model using the full-profile analysis software FullProf Suite. The diffraction pattern fitting within the structural data of the two phases revealed that the analyzed layers could be described by FCC phases with lattice parameters of 0.3692 nm and 0.3633 nm. The ratio of phase quantity was 14 and 86 vol. %, respectively.

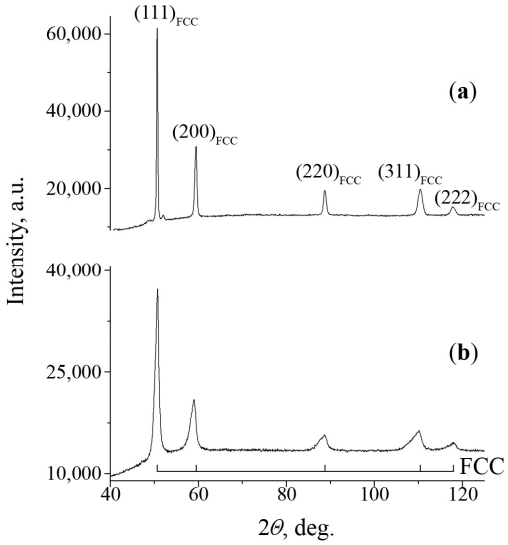


Figure 5. X-ray diffraction patterns of $FeMn_{22}Cr_{18}N_{0.83}$ steel surface, registered in Co-Kα radiation. Treatment: (**a**)—aging 800 °C, 30 h; (**b**)—aging 800 °C, 30 h and friction.

3.2. Analysis of the Wear Product Structure in the Quenched and Aged Steel Friction

The structure of wear products of $FeMn_{22}Cr_{18}N_{0.83}$ steel is shown in Figure 6. The powdered samples consist of particles represented by flakes with distribution by sizes and variation by shapes. Besides coarse particles with a size of 500 µm or greater, it was possible to register much smaller ones seen by transmission electron microscopy, as shown in Figure 7a,b. It was interesting to observe the regular rectangular shape of fine nanoparticles. Dark-field images of dispersed particles from the wear products in reflection $(002)_{Fe16N2}$ are shown in Figure 7c,d.

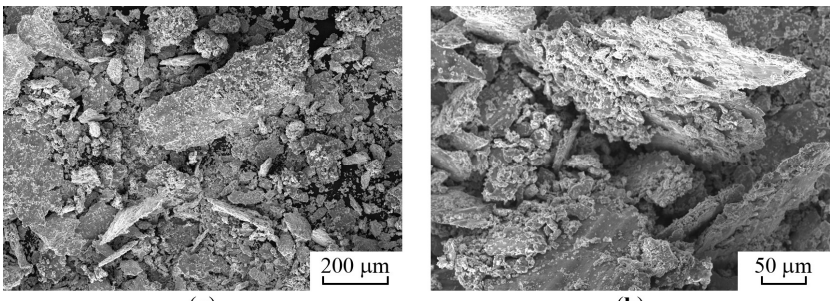


Figure 6. SEM images of particles in the powdered wear products of the $FeMn_{22}Cr_{18}N_{0.83}$ steel (**a**,**b**).

The Mössbauer spectra of wear products of aged alloys revealed a central line related to austenite and an additional developing sextet with integral intensity up to 30% associated with a ferromagnetic structure, namely, strain-induced martensite (see Figure 8).

Increasing the time of preaging from 2 to 30 h results in austenite destabilizing and an integral intensity growth of up to 30% for the sextet related to martensite. A thorough analysis of the Mössbauer spectrum and the effective magnetic field ($p(H)$) distribution of the ferromagnetic part in the wear products allowed extracting components associated with iron and nitrogen atoms in the second coordination spheres of solid solution α′-Fe–N (sextet A') and nitride α″-$Fe_{16}N_2$ (sextet II) [17,18] (see Figure 8). Other spectral components of solid solution α′-Fe–N and nitride α″-$Fe_{16}N_2$ were overlapped with the components from substitutional elements Mn and Cr in the martensite ferromagnetic structure of the steel wear products. The Mössbauer results reflecting the presence of $Fe_{16}N_2$ nitrides in the wear products of $FeMn_{22}Cr_{18}N_{0.83}$ steel were supported by X-ray structural analysis data. The X-ray patterns of the wear products in the samples aged at 800 °C for 2 and 30 h are shown

in Figure 9. The presence of the austenite phase together with the reflections of the nitride structure α''-$Fe_{16}N_2$ was evident.

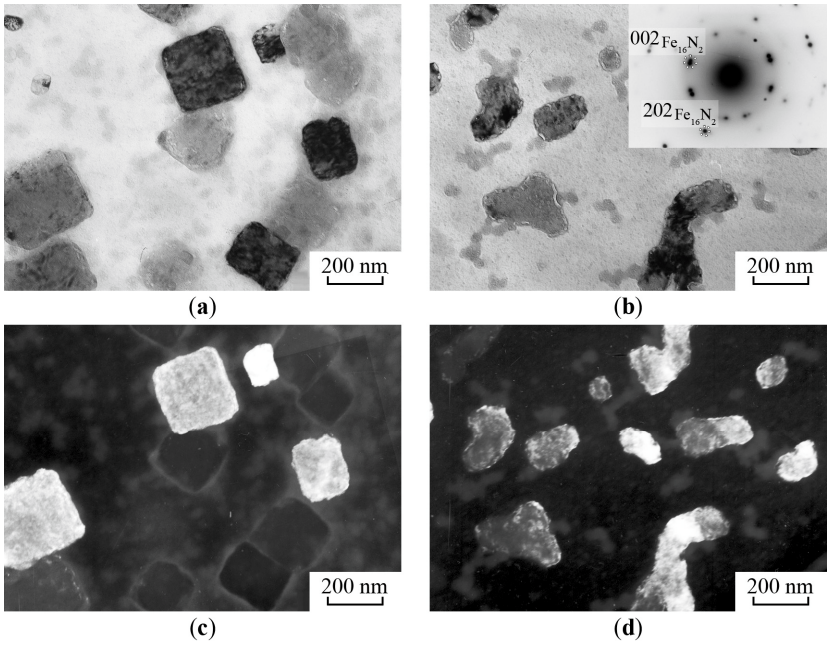


Figure 7. Electron microscopy of the wear product in the $FeMn_{22}Cr_{18}N_{0.83}$ steel. (**a**,**b**)—Bright-field images and SAED pattern; (**c**,**d**)—dark-field images of (**a**,**b**), registered in reflection $(002)_{Fe16N2}$.

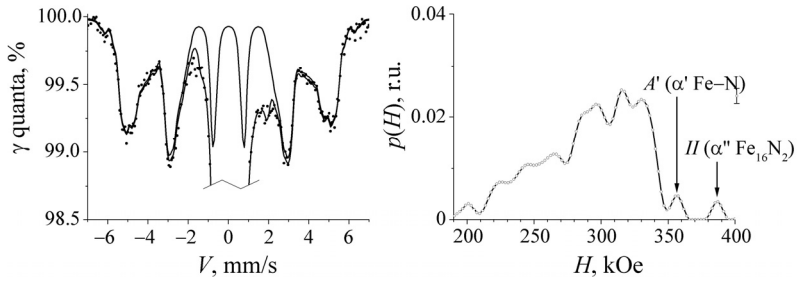


Figure 8. Mössbauer spectrum and $p(H)$distribution of the wear product in the $FeMn_{22}Cr_{18}N_{0.83}$ steel within the velocity region of α-Fe after quenching from 1150 °C and further aging at 800 °C for 30 h.

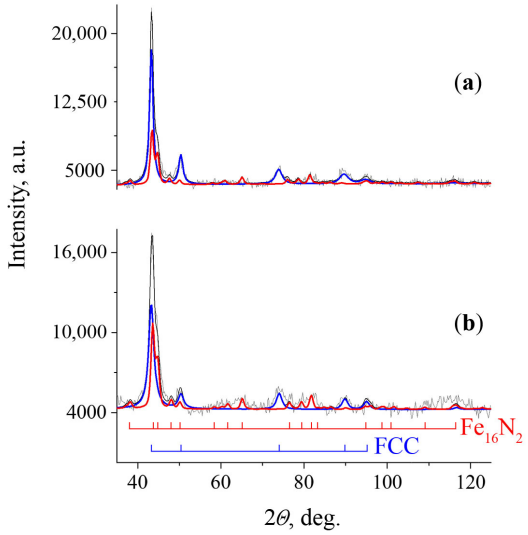


Figure 9. X-ray diffraction patterns of wear products in the $FeMn_{22}Cr_{18}N_{0.83}$ steel registered in Cu-Kα radiation. Treatment: (**a**)—aging 800 °C, 30 h; (**b**)—aging 800 °C, 30 h, and friction.

The Mössbauer spectra of the wear products of the quenched and aged samples revealed significant variation in the central singlet line shape associated with austenite, as shown in Figure 10.

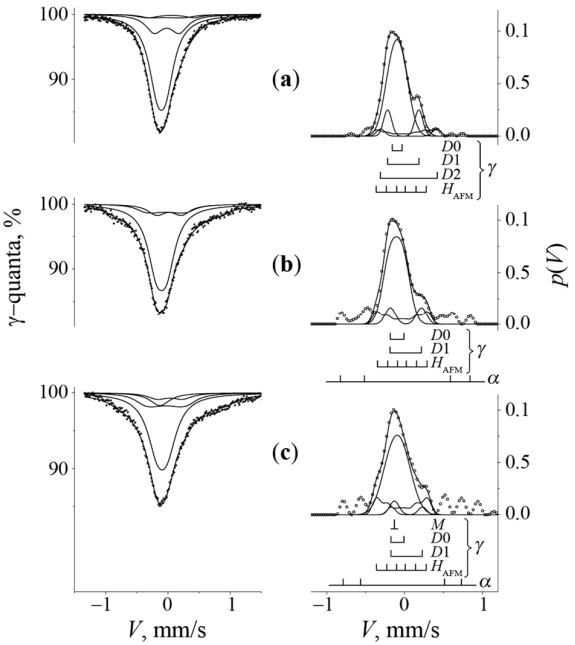


Figure 10. Mössbauer spectra and $p(V)$ distributions of the wear products in the quenched and aged $FeMn_{22}Cr_{18}N_{0.83}$ steel. Preliminary treatment: (**a**)—quenching from 1150 °C; (**b**)—aging 800 °C, 2 h; (**c**)—aging 800 °C, 30 h.

Further measurements of the spectrum central region characterizing austenite with a higher resolution demonstrated substantial broadening and $p(V)$ distribution, indicated by the presence of the additional antiferromagnetic component H_{AFM}, as shown in Figure 10. The analysis and modeling of the spectra from wear products in the steel were performed based on the hyperfine structure of binary Fe–Mn alloys and ternary Fe–Mn–Cr ones [19–22]. This decision can be verified by the fact that polymorphic transformations with the development of γ-, α-, and ε-phases, as well as antiferromagnetic ordering in austenite, can take place in alloys with similar composition. The antiferromagnetic ordering in $Fe_{80}Mn_{20}$ alloys and mechanically synthesized mixtures of Fe + 20% Mn_2N and $FeCr_{15}$ + 20% Mn_2N can be explained by the formation of regions in the austenite structure with a Neel temperature higher than room temperature at which the spectra measurements were performed [19], as shown in Figure 11. Thus, spectra modeling with discrete decomposition should take into account the component of the poorly resolved magnetic sextet with an effective field value H_{AFM} of ~21 kOe related to the antiferromagnetic austenite (see Figures 10 and 11 and Table 1). Moreover, sometimes, in order to improve spectra decomposition for the strain-induced alloys, an additional single-line component M was added with an isomer shift displaced to negative values on the velocity scale in relation to the central component $D0$, as shown in Figure 10c. The I_s value of this single line is similar to that of either the ε-phase or disordered stacking faults, which are multiple ε-phase nuclei [22–24].

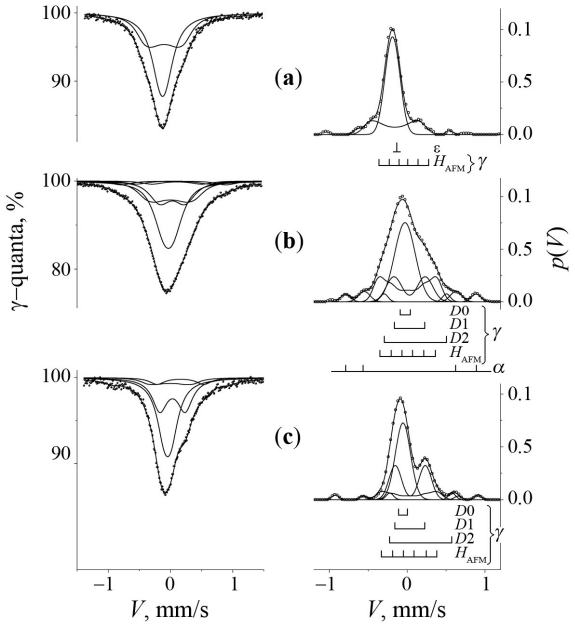


Figure 11. Mössbauer spectra and $p(V)$ distributions. (**a**)—The $FeMn_{20}$ alloy; (**b**)—mechanically synthesized mixture of Fe + 20%Mn_2N in the ball mill; (**c**)—mechanically synthesized mixture of $Fe_{85}Cr_{15}$ + 20%Mn_2N in the ball mill [19].

4. Discussion

The results of the Mössbauer study demonstrated that the phase composition of the 20–25 μm surface layers in the quenched and aged steels after dry sliding friction was saved. The spectrum of the aged steel demonstrated growth in *D*1 partial contribution, reflecting some nitrogen return from nitrides to an austenite matrix, as shown in Figure 3b′,c′ and Table 1. This idea was proven by the X-ray data (see Figure 5). Sliding caused sample deformation under shear and elastic stresses. On the front side of the counterbody, the contact zone of the sample material was strained under the simultaneous influence of shear and compression stresses (see Figure 1). The results of the friction effect on the steel surface layers were similar to those under the conditions of high-pressure torsion in rotating Bridgeman anvils. This fact confirmed the formation of conditions with severe plastic deformation and compression on the front side of the indentor during the dry sliding friction treatment (Figure 1). Thus, the latter activates atomic mass transfer in the form of nitride dissolution in the metal matrix at relatively low temperatures ($T < 0.2\ T_{melt.}$) [7,10,25–29].

Stretching contact stresses on the back side of the contact zone activated the processes of material degradation and α-martensite formation in the wear products. The amount of strain-induced martensite grew with increased time of preaging and decreased the nitrogen and chromium content in the austenite. A decrease in the nitrogen and chromium contents in the austenite structure of wear products was revealed as the antiferromagnetic ordering of austenite, as shown in Figure 8. Using CEMS on the ~0.1 μm surface layer of the aged steel damaged by friction also supported the appearance of antiferromagnetic austenite (see Figure 4). According to the magnetic phase diagram, the antiferromagnetic ordering of Fe–Mn–Cr alloys occurs as the chromium content in austenite decreases [20]. Additional nitrogen and chromium depletion in the ~0.1 μm surface layers and wear products might result from dynamic aging accelerated by direct heating in the true contact zone of material microvolumes. Similar accelerated dynamic aging has already been observed for nitrogen-bearing austenitic steels during grinding in a ball mill due to the increased local temperature of the material caused by ball strokes [19,30]. In ref. [25], it was also shown that, in $FeMn_{22}Cr_{18}N_{0.83}$ steel exposed to high-pressure torsion at $T \geq 100$ °C, the process of mechanical alloying was accompanied by austenite degradation with major chromium and nitrogen release into the secondary CrN nitrides. Thus, the antiferromagnetic phase

transition and austenite destabilization in the surface layers (~0.1 μm) and wear products might result from accelerated strain-induced aging. Similar antiferromagnetic ordering was observed in mechanically synthesized model alloys obtained by grinding a mixture of Fe + 20% Mn_2N and $FeCr_{15}$ + 20% Mn_2N in the ball mill due to austenite formation with a Mn content of ~20% and a Neel temperature higher than room temperature [19], as shown in Figure 11. When aged $FeMn_{22}Cr_{18}N_{0.83}$ steel was exposed to friction, the phase and concentration compositions of wear products developed due to the mechanical alloying of the composite material represented by the initial austenite Fe–Mn–Cr and pearlite-like assemblies of Cr_2N nitrides. Thus, the exposure realized in the steel surface layers close to the friction contact zone was similar to mechanical alloying in the ball mill. Both mentioned methods of mechanical synthesis result in the development of inhomogeneous regions of austenite structures with manganese retention but accelerated chromium and nitrogen release into secondary nitrides [19,30]. Structural peculiarities of the wear products were manifested in the conversion electron Mössbauer spectra of the 0.1 μm surface layers of the aged steel subjected to friction. This was mainly related to the formation of antiferromagnetic austenite components (see Figure 4). However, the conversion electron Mössbauer spectra revealed no, or a tiny amount of, sextet associated with strain-induced martensite. This fact confirmed the existence of stretching stresses on the backside of the indentor, activating $\gamma \rightarrow \alpha$ transformation and structure relaxation in the form of α'-martensite and α''-$Fe_{16}N_2$ nitride development.

The wearing of aged $FeMn_{22}Cr_{18}N_{0.83}$ steel results in the formation of an α''-$Fe_{16}N_2$ structure, which is of great interest for independent study as a material with peculiar magnetic properties [31–33]. The well-known basic procedure to obtain nitride α''-$Fe_{16}N_2$ is the quenching of nitrided austenite at temperatures below 0 °C to form α'-Fe–N martensite, with further annealing at 120 °C [34]. Other techniques for the cultivation of α''-$Fe_{16}N_2$ structures mostly refer to film technologies, like epitaxy, magnetron sputtering, nitrogen implantation, etc. [33]. In 2016, Jiang et al. offered to produce α''-$Fe_{16}N_2$ by means of stretching stresses (for the elongation of a martensite crystal lattice) and the low annealing of wire [35]. In the case of film technologies, stretching stresses are executed on the substrate and promote α''-$Fe_{16}N_2$ formation. The development of α''-$Fe_{16}N_2$ nitride structures has already been seen in experiments with the mechanical synthesis of nitrogenized layers in BCC iron using ion plasma techniques [18]. An experiment was performed on sandwich-like samples consisting of a number of iron foils containing Fe_4N nitrides created on an α-Fe surface. The mechanical alloying of sandwich-like samples was performed in rotating Bridgman anvils. Mechanically synthesized α''-$Fe_{16}N_2$ nitrides appear according to the following reactions: Fe_4N + α-Fe → γ-Fe–N + α'-Fe–N + α''-$Fe_{16}N_2$. The moderate heating of mechanically synthesized samples containing γ-Fe–N, α'-Fe–N, and α''-$Fe_{16}N_2$ increases the amount of α''-$Fe_{16}N_2$ structures, owing to the solid solution of α'-Fe–N. The formation of α''-$Fe_{16}N_2$ in the current study took place during the $\gamma \rightarrow \alpha$ martensite phase transition process in the steel surface layers and was accompanied by stretching stresses in the friction contact zone. The development of α''-$Fe_{16}N_2$ is also promoted by moderate temperature increases in surface irregularities, which are local regions of contact stresses under frictional conditions [25,34,35]. The specific morphology of fine particles in the wear products presented by crystallites with regular rectangular shapes might result from the ordering during the formation of nanocrystalline α''-$Fe_{16}N_2$ nitrides.

5. Conclusions

The influence of dry sliding friction on the structure of the surface layers and wear products of the austenite $FeMn_{22}Cr_{18}N_{0.83}$ steel was studied using Mössbauer spectroscopy, X-ray structural analysis, and electron microscopy. The obtained results regarding structural phase transformations in the form of mechanical alloying and polymorphic $\gamma \rightarrow \alpha$ phase transitions in the region of friction contact confirmed previously obtained data regarding the conditions of severe plastic deformation similar to those in rotating Bridgeman anvils and ball mills.

The structure analysis in the region of adhesion contact revealed the following results:

- The contact stresses in the region of tribological exposure resulted in a nanostructure formation with gradient phase and concentration composition in the steel surface layers.
- The Cr_2N nitride phase particles were found to dissolute in the austenite matrix at the depth of 20–25 microns, thereby increasing nitrogen content in the solid solution state due to compressive stresses that occurred in the surface layers.
- The regions of antiferromagnetic austenite with decreased chromium and nitrogen content in the metal matrix were caused by dynamical aging accelerated by local heating in the thin surface layers (0.1 microns) of friction contact and the wear products.
- Stretching stresses in the friction contact zone destabilized the austenite and broke down the sample surface layers, thereby generating wear products. Wear products were represented by nanostructural powder, the phase composition of which revealed nitrogen-depleted austenite, nitrous martensite, and nanocrystalline α''-$Fe_{16}N_2$ nitrides.

Author Contributions: Conceptualization, V.S. and L.K.; methodology, V.S., L.K., K.K., K.L., A.Z., G.D. and N.K.; validation, V.S. and L.K.; formal analysis, A.Z., G.D. and N.K.; investigation, K.K., K.L., G.D. and N.K.; visualization, A.Z., K.K. and N.K.; writing—original draft preparation, V.S.; writing—review and editing, V.S., K.K. and K.L.; project administration, V.S. All authors have read and agreed to the published version of the manuscript.

Funding: The research was carried out within the state assignment of the Ministry of Science and Higher Education of the Russian Federation (theme structure no.: 122021000033-2).

Data Availability Statement: Not applicable.

Acknowledgments: Mössbauer, electron-microscopic, and X-ray diffraction studies were performed in the Mössbauer spectroscopy, Electron Microscopy, and X-ray diffraction analysis Departments of the Collective Usage Center at the M.N. Mikheev Institute of Metal Physics, Ural Division, Russian Academy of Sciences.

Conflicts of Interest: The authors declare no conflict of interest.

References

1. Howell, P.K.; Nilsson, J.O.; Horswell, A.; Dunlop, G.L. The formation of multipoles during high-temperature creep of austenite stainless steel. *J. Mater. Sci.* **1981**, *16*, 2860–2866. [CrossRef]
2. Korshunov, L.G.; Chernenko, N.L.; Tereshchenko, N.A.; Uvarov, A.I. Effect of aging on the tribologic and mechanical properties of a high-nitrogen stainless austenitic steel. *Phys. Met. Metallogr.* **2005**, *99*, 90–99.
3. Korshunov, L.G.; Shabashov, V.A.; Chernenko, N.L.; Pilyugin, V.P. Influence of the stressed state of the zone of friction contact on the formation of the structure of a surface layer and tribological properties of steels and alloys. *Phys. Met. Metallogr.* **2008**, *105*, 64–78. [CrossRef]
4. Qiao, Y.-X.; Sheng, S.-L.; Zhang, L.-M.; Chen, J.; Yang, L.-L.; Zhou, H.-L.; Wang, Y.-X.; Li, H.-B.; Zheng, Z.-B. Friction and wear behaviors of a high nitrogen austenitic stainless steel Fe-19Cr-15Mn-0.66N. *J. Min. Metall. Sect. B-Metall.* **2021**, *7*, 285–293. [CrossRef]
5. Mao, B.; Chu, S.; Wang, S. Effect of grain size on the friction-induced martensitic transformation and tribological properties of 304 austenite stainless steel. *Metals* **2020**, *10*, 1246. [CrossRef]
6. Grabco, D.; Pyrtsac, C.; Topal, D.; Shikimaka, O. Effect of friction on the micromechanical properties of AISI 316L austenitic steel. *J. Eng. Sci.* **2021**, *XXVIII*, 34–43. [CrossRef]
7. Glezer, A.M.; Metlov, L.S. Physics of megaplastic (severe) deformation in solids. *Phys. Solid State* **2010**, *52*, 1162–1169. [CrossRef]
8. Shabashov, V.A.; Korshunov, L.G.; Zamatovskii, A.E.; Litvinov, A.V.; Sagaradze, V.V.; Kositsyna, I.I. Deformation-induced dissolution of carbides of the Me(V, Mo)-C type in high-manganese steels upon the friction effect. *Phys. Met. Metallogr.* **2012**, *113*, 914–921. [CrossRef]
9. Korshunov, L.G.; Sagaradze, V.V.; Chernenko, N.L.; Shabashov, V.A. Friction-induced structural transformations of the carbide phase in Hadfield steel. *Phys. Met. Metallogr.* **2015**, *116*, 823–828. [CrossRef]
10. Shabashov, V.A.; Korshunov, L.G.; Sagaradze, V.V.; Kataeva, N.V.; Zamatovsky, A.E.; Litvinov, A.V.; Lyashkov, K.A. Mossbauer analysis of deformation dissolution of the products of cellular decomposition in high-nitrogen chromium manganese austenite steel. *Philos. Mag.* **2014**, *94*, 668–682. [CrossRef]
11. Korshunov, L.G.; Goikhenberg, Y.N.; Chernenko, N.L. Effect of discontinuous decomposition on the tribologic properties of high-nitrogen chromium manganese austenitic steel G22Kh18A0.80. *Phys. Met. Metallogr.* **2000**, *90*, 192–198.

12. Shabashov, V.A.; Korshunov, L.G.; Sagaradze, V.V.; Litvinov, A.V.; Zamatovsky, A.E. Mössbauer analysis of nitride and carbide dissolution in austenitic high-manganese steels under conditions of friction. *Bull. Russ. Acad. Sci. Phys.* **2013**, *77*, 803–806. [CrossRef]
13. Rusakov, V.S.; Kadyrzhanov, K.K. Mössbauer spectroscopy of locally inhomogeneous systems. *Hyperfine Interact.* **2005**, *164*, 87–97. [CrossRef]
14. Renot, R.C.; Swartzendruber, L.J. Origin of Mössbauer linewidth in stainless steel. *AIP Conf. Proc.* **1973**, *10*, 1350–1353. [CrossRef]
15. Srivastava, B.P.; Sarma, H.N.K.; Bhattacharya, D.L. Quadrupole splitting in deformed stainless steel. *Phys. Status Solidi A* **1972**, *10*, K117–K118. [CrossRef]
16. Oda, K.; Umezu, K.; Ino, H. Interaction and arrangement of nitrogen atoms in FCC γ-iron. *J. Phys. Condens. Matter* **1990**, *2*, 10147–10158. [CrossRef]
17. Moriya, T.; Sumitomo, Y.; Ino, H.; Fujita, F.E.; Maeda, Y. Mossbauer effect in iron-nitrogen alloys and compounds. *J. Phys. Soc. Jpn.* **1973**, *35*, 1378–1385. [CrossRef]
18. Shabashov, V.A.; Borisov, S.V.; Zamatovsky, A.E.; Vildanova, N.F.; Mukoseev, A.G.; Litvinov, A.V.; Shepatkovsky, O.P. Deformation-induced transformations in nitride layers formed in bcc iron. *Mat. Sci. Eng. A* **2007**, *452–453*, 575–583. [CrossRef]
19. Lyashkov, K.; Shabashov, V.; Zamatovskii, A.; Kozlov, K.; Kataeva, N.; Novikov, E.; Ustyugov, Y. Structure-phase transformations in the course of solid-state mechanical alloying of high-nitrogen chromium-manganese steels. *Metals* **2021**, *11*, 301. [CrossRef]
20. Pepperhoff, W.; Acet, M. *Constitution and Magnetism of Iron and its Alloys*; Springer: Berlin/Heidelberg, Germany, 2001.
21. Endoh, Y.; Ishikawa, Y. Antiferromagnetism of iron manganes alloys. *J. Phys. Soc. JPN* **1971**, *30*, 1614–1627. [CrossRef]
22. Amigud, G.P.; Bogachevv, I.N.; Dorofeev, G.A. Study of iron-manganese austenitic alloys by nuclear gamma resonance. *Phys. Met. Metallogr.* **1973**, *36*, 666–668. (In Russian)
23. Trichter, F.; Rabinkin, A.; Ron, M.; Sharfstein, A. A study of $\gamma \rightarrow \varepsilon$ phase transformation in Fe-Mn alloys induced by high pressure and plastic deformation. *Scr. Metall.* **1978**, *12*, 431–434. [CrossRef]
24. Zeeger, A. Verzetzungen und allotrope umwandlungen. *Int. J. Mater. Res.* **1953**, *44*, 247–253. [CrossRef]
25. Shabashov, V.; Lyashkov, K.; Kozlov, K.; Zavalishin, V.; Kataeva, N.; Sagaradze, V.; Ustyugov, Y. Critical redistribution of nitrogen in the austenitic Cr–Mn steel under severe plastic deformation. *Materials* **2021**, *14*, 7116. [CrossRef] [PubMed]
26. Sagaradze, V.V.; Shabashov, V.A. Anomalous diffusion phase transformations in steels upon severe cold deformation. *Phys. Met. Metallogr.* **2011**, *112*, 146–164. [CrossRef]
27. Duan, J.; Wen, H.; Zhou, C.; He, X.; Islamgaliev, R.; Valiev, R. Annealing behavior in a high-pressure torsion-processed Fe–9Cr steel. *J. Mater. Sci.* **2020**, *55*, 7958–7968. [CrossRef]
28. Čížek, J.; Janeček, M.; Srba, O.; Kužel, R.; Barnovská, Z.; Procházka, I.; Dobatkin, S. Evolution of defects in copper deformed by high-pressure torsion. *Acta Mater.* **2011**, *59*, 2322–2329. [CrossRef]
29. Shabashov, V.A.; Kozlov, K.; Ustyugov, Y.; Zamatovskii, A.; Tolmachev, T.; Novikov, E. Mössbauer Analysis of Deformation–Induced Acceleration of Short-Range Concentration Separation in Fe-Cr Alloys—Effect of the Substitution Impurity: Sb and Au. *Metals* **2020**, *10*, 725. [CrossRef]
30. Shabashov, V.; Lyashkov, K.; Zamatovskii, A.; Kozlov, K.; Kataeva, N.; Novikov, E.; Ustyugov, Y. Mechanosynthesis of high-nitrogen steels strengthened by secondary titanium nitrides. *Materials* **2022**, *15*, 5038. [CrossRef]
31. Abdellateef, M.A.; Heiden, C.; Lemke, H.; El-Hossary, F.M.; Baerner, K. Magnetic properties and structure of the α″-Fe16N2 films. *J. Magn. Magn. Mater.* **2003**, *256*, 214–220. [CrossRef]
32. Feng, L.; Zhang, D.; Wang, F.; Dong, L.; Chen, S.; Liu, J.; Hui, X. A new structure of the environment-friendly material Fe16N2. *Chem. Eng. Trans.* **2017**, *61*, 1501–1506. [CrossRef]
33. Wojciechowski, P.; Lewandowski, M. Iron nitride thin films: Growth, structure, and properties. *Cryst. Growth Des.* **2022**, *22*, 4618–4639. [CrossRef] [PubMed]
34. Jack, K.H. The synthesis and characterization of bulk α''-$Fe_{16}N_2$. *J. Alloys Compd.* **1995**, *22*, 160–166. [CrossRef]
35. Jiang, Y.; Dabade, V.; Allard, L.F.; Lara-Curzio, E.; James, R.; Wang, J.P. Synthesis of α″-Fe16N2 compound anisotropic magnet by the strained-wire method. *Phys. Rev. Appl.* **2016**, *6*, 024013. [CrossRef]

Disclaimer/Publisher's Note: The statements, opinions and data contained in all publications are solely those of the individual author(s) and contributor(s) and not of MDPI and/or the editor(s). MDPI and/or the editor(s) disclaim responsibility for any injury to people or property resulting from any ideas, methods, instructions or products referred to in the content.